BJR

Received: 9 May 2016 | Revised: 28 September 2016 | Accepted: 10 November 2016

https://doi.org/10.1259/bjr.20160402

Cite this article as:
Ljungberg M, Pretorius PH. SPECT/CT: an update on technological developments and clinical applications. *Br J Radiol* 2018; **90**: 20160402.

NUCLEAR MEDICINE: PHYSICS AND INSTRUMENTATION SPECIAL FEATURE REVIEW ARTICLE

SPECT/CT: an update on technological developments and clinical applications

[1]MICHAEL LJUNGBERG, PhD and [2]P HENDRIK PRETORIUS, PhD

[1]Department of Medical Radiation Physics, Lund University, Lund, Sweden
[2]Division of Nuclear Medicine, Department of Radiology, University of Massachusetts Medical School, Worcester, MA, USA

Address correspondence to: Professor Michael Ljungberg
E-mail: *michael.ljungberg@med.lu.se*

ABSTRACT

Functional nuclear medicine imaging with single-photon emission CT (SPECT) in combination with anatomical CT has been commercially available since the beginning of this century. The combination of the two modalities has improved both the sensitivity and specificity of many clinical applications and CT in conjunction with SPECT that allows for spatial overlay of the SPECT data on good anatomy images. Introduction of diagnostic CT units as part of the SPECT/CT system has also potentially allowed for a more cost-efficient use of the equipment. Most of the SPECT systems available are based on the well-known Anger camera principle with NaI(Tl) as a scintillation material, parallel-hole collimators and multiple photomultiplier tubes, which, from the centroid of the scintillation light, determine the position of an event. Recently, solid-state detectors using cadmium–zinc–telluride became available and clinical SPECT cameras employing multiple pinhole collimators have been developed and introduced in the market. However, even if new systems become available with better hardware, the SPECT reconstruction will still be affected by photon attenuation and scatter and collimator response. Compensation for these effects is needed even for qualitative studies to avoid artefacts leading to false positives. This review highlights the recent progress for both new SPECT cameras systems as well as for various data-processing and compensation methods.

INTRODUCTION

The single-photon emission CT (SPECT)/CT combination of dual-imaging modality techniques is a clinical application that when introduced was particularly relevant in oncological applications, as it leads to improved sensitivity and specificity by the combination of co-registered anatomical and functional images.[1] When evaluating treatment outcome, the combination of the two modalities may also lead to improved staging and treatment monitoring.

Prior to SPECT/CT, most manufactures offered transmission imaging using scanning line sources, scanning point sources, a single static line source or multiple static line sources. These systems were used to form maps of linear attenuation coefficients for attenuation compensation[2] and lack the resolution and overall quality for anatomic registration and other applications. The need for more rapidly acquired and more accurate attenuation maps as well as localization capabilities led to the development of SPECT/CT.

One such application where anatomical information was found to be needed was in the diagnostic imaging of tumours. In many situations, the tumour uptake of the radiopharmaceutical can be high compared with normal organs, making it difficult to localize the tumour potential future surgery. Anatomic landmarks in SPECT images are generally inadequate to accurately determine the locations of the malignancies. This was of course recognized and research on rigid and non-rigid image registration between SPECT and CT were conducted, but the task of doing this accurately demands sophisticated mathematical algorithm and even when a diagnostic CT was available, the matching of the images was not always successful owing to organ displacement between the studies. The solution was then a combined SPECT/CT system designed in such a way that when translating the patient between the two modalities patient movements was avoided. These so-called hybrid systems then made fusion of SPECT and CT images possible for clinically routine procedures.

THE EVOLUTION OF COMBINED SINGLE-PHOTON EMISSION CT AND CT SYSTEM

The first commercial SPECT/CT combination that was designed as a single unit was the GE Millenium™ hybrid SPECT/positron emission tomography (PET)/CT camera equipped with the HawkEye™ single-slice CT (GE Healthcare, Haifa, Israel). The CT produced images with a slice thickness of 1 cm and a 256×256 matrix size with a spatial resolution of about 3.5 mm. Owing to course resolution, the unit was not regarded as a diagnostic CT. An acquisition that matched the field of view (FOV) for the SPECT cameras took approximately 10 min to complete. Reconstruction was performed using filtered back-projection. The system was also offered with a 1-inch crystal and a coincidence unit for PET imaging, since at that time SPECT-based PET imaging without collimation was marketed as a more economical alternative to dedicated PET systems. This system was the commercial implementation of the very successful research by the late Hasegawa et al.[3,4] Current SPECT/CT systems, offered by Philips Healthcare, General Electric (GE) Healthcare, Mediso Medical Systems and Siemens Medical Solutions, all offer high-resolution diagnostic CT units as part of their SPECT/CT systems. Mediso even offer a complete SPECT/CT/PET with high-resolution Lutetium-yttrium oxyorthosilicate (LYSO) detector technology as part of their AnyScan family of systems.

FUSION OF FUNCTIONAL AND ANATOMICAL INFORMATION

The fusion of anatomical and functional images requires inherent registration to each other, meaning a particular voxel number *i,j,k* in a SPECT image set represents the same location *i,j,k* in the CT images. Before the introduction of combined SPECT/CT systems, the registration was accomplished by mathematical methods using landmarks (mutual information) in the SPECT and the CT image set. For these algorithms to successfully register data, it was important that the patient positioning and posture were essentially identical to avoid situations that required non-rigid transformations.

In most cases, the spatial resolution of CT images is much better than that of SPECT images and therefore, resampling of SPECT images by interpolation methods is required to match the voxel size of the CT images. It should be noted that image registration might still be necessary to correct slight motion/shifts between acquisitions. Furthermore, for dosimetry studies where several SPECT/CT studies are performed in order to obtain time–activity curves, the separate SPECT and CT images might not be registered by the system hardware, since the patient has been repositioned several times. The ideal is to acquire a SPECT/CT scan at each time point; however, even low-dose attenuation maps could be used to great advantage in performing the registration to a higher resolution diagnostic CT.

SCALING OF CT DATA TO PHYSICAL UNITS

The information obtained from a CT system is turned into Hounsfield units (HUs) defined as $HU = 1000\ (\mu - \mu_{water})/(\mu_{water} - \mu_{air})$, where μ is the linear attenuation coefficient, a function of photon energy, tissue composition and tissue density. The reference material is water at a standard pressure and temperature, while μ in turn can be expressed as a product of the mass attenuation coefficient μ_m and the tissue density ρ (μ_m/ρ). Mass attenuation coefficients can be found in databases maintained by the National Institute of Standards and Technology.[5] Since μ_m reflects the electron density, scaling to physical density ($g\,cm^{-3}$) generally needs a calibration against a phantom of different materials. It is important to remember that the scaling also depends on the X-ray tube voltage used in a particular study. If the density distribution can be obtained with acceptable accuracy, this can then be used to create so-called attenuation maps for use in attenuation correction methods. For a particular photon energy, the scaling required to produce the attenuation maps is straightforward. However, HUs are generated using a continuous energy spectrum of photons and thus, where this changes, *e.g.* obese subjects, through loss of low-energy photons due to absorption, the HUs will be different from those of smaller patients—this needs correction.

SINGLE-PHOTON EMISSION CT/CT ACQUISITION

Most clinical SPECT systems still rely on the Anger camera principle, where the location of a photon interaction (*i.e.* scintillation) site is calculated as the centre of gravity of the position-dependent energy signals from a two-dimensional (2D) array of photomultiplier tubes (PMTs) attached to the back of the scintillation crystal.[6] The available NaI(Tl) crystal thicknesses vary between 3/8 and 3/4 inch (9.5 and 19 mm) depending upon the intended usage for low radionuclides emitting lower energy photons (*e.g.* ^{99m}Tc) and higher energy photons (*e.g.* ^{131}I). Thicker crystals improve the photo-peak efficiency but degrade the intrinsic spatial resolution. The 1-inch (2.54 mm) cut crystal offered by GE in the early 2000s (StarBright™) is not available any more. This crystal had thin cuts made to form blocks that acted as light guides. The purpose was to reduce the degradation of the intrinsic spatial resolution that otherwise would have been the result owing to the thickness of the crystal. Although this crystal was predominantly used in the earlier coincidence PET gamma cameras to efficiently absorb the 511-keV photons, it also significantly improved the sensitivity for higher energy radionuclides such as ^{131}I and ^{111}In imaging by decreasing the transmitted fraction of photons.

The current SPECT systems are equipped with detection devices to automatically calculate non-circular orbits: The detection methods can be based on optical detection using light-emitting diodes or electromagnetic signals generated by the collimators. Aside from the safety aspect, non-circular orbits ensure closer distances to the patient for each of the SPECT projections as well as easy setup procedures, which together reduce the overall time that the patient spends on the imaging table. However, the additional motions between projections to position camera heads can again add to the overall study time.

Parallel-hole collimators with hex-shaped holes of different hole diameters, hole lengths and septum thicknesses are generally used for SPECT imaging. The design depends on required resolution/sensitivity and the energy of the photons. Although other manufacturers previously offered collimators dedicated to specific imaging protocols (Cardio-Focal by Picker, now Philips), Siemens now offers a similar collimator for cardiac

perfusion imaging, called Smart Zoom, where the central portion focuses on the heart and collects up to a factor of four times more counts than conventional parallel-hole collimators. Whereas the cardiofocal collimator only magnifies and improves the count statistics in the heart region while truncating the rest of the body, the Smart Zoom collimators magnify the heart region while still acquiring counts up to the body edge for a large range of patient body sizes. Truncation is thus greatly reduced. Their camera also utilizes a cardiocentric orbit where the user centres the camera on the heart instead of the mechanical centre of the camera. This improved orbit ensures that the heart remains in the magnification area of the Smart Zoom collimator. It is envisaged that more such dedicated imaging solutions will become available in the near future.

GE and Siemens offer advanced and integrated diagnostic SPECT/CT solutions with 2-, 6- or 16-slice diagnostic CTs. Basically, the SPECT/CT is a hybrid or a combination of each of the two systems that have the same characteristics as the respective standalone devices. A similar offer from Philips was discontinued.

Philips, with the BrightView XCT system, added a dedicated flat-panel low-dose cone-beam CT (CBCT) for localization and attenuation correction to their two-headed SPECT cameras (Figure 1). The flat-panel detector is mounted on the same gantry as the SPECT cameras, enabling coplanar SPECT and CBCT. The CT flat-panel detector (40×30 cm) is mounted at a lateral offset with respect to the X-ray tube. An X-ray projection covers slightly more than half of the CT FOV. With a 360° rotation of the gantry, a 47-cm diameter transverse FOV and a 14.4-cm axial length along the patient can be imaged. The system provides reconstructed images with a 1-mm isotropic voxel size for the entire FOV and as small as a 0.33-mm isotropic voxel size for high-resolution subvolume reconstructions. Either 300 or 720 X-ray projections can be acquired during a full rotation with 12-, 24- or 60-s rotation times.

IMAGE RECONSTRUCTION AND QUANTIFICATION USING ANATOMICAL INFORMATION

Image reconstruction

Most of the newer SPECT systems have the option to select statistical iterative reconstruction for creating images.[7,8] Briefly, an iterative procedure includes some kind of model of how the images are formed by the acquisition system. For a SPECT system, an image is formed by the collimation of emitted photons in such a way that only those photons having a direction within a cone-shaped volume, formed by the collimator holes that are orthogonal to the crystal surface, will interact with the crystal and produce scintillation events. Thereby, these so-called projections are created as 2D representations of all photons detected along the projection cones and this give rise to a distance-dependent resolution. Thus, no source depth information exists in the 2D projections and it is therefore the purpose of the reconstruction algorithm to create an estimate of the source distribution in 3D. From the CT in SPECT/CT systems, attenuation maps are generated and incorporated in the image formation model.

Figure 1. Cardiac perfusion stress single-photon emission CT (SPECT)/CT images of a 51-year-old female with a body mass index of 38.1 kg/m2 acquired on a BrightView (Philips Medical, Cleveland, OH) equipped with a low-dose cone-beam CT: the top row is showing the registration between SPECT and CT in three orientations (transaxial, coronal and sagittal), while the subsequent rows are demonstrating the improvement when attenuation, scatter and spatial resolution corrections are performed. The arrows on the filtered backprojection slices are pointing to a decrease in apparent uptake due to breast attenuation.

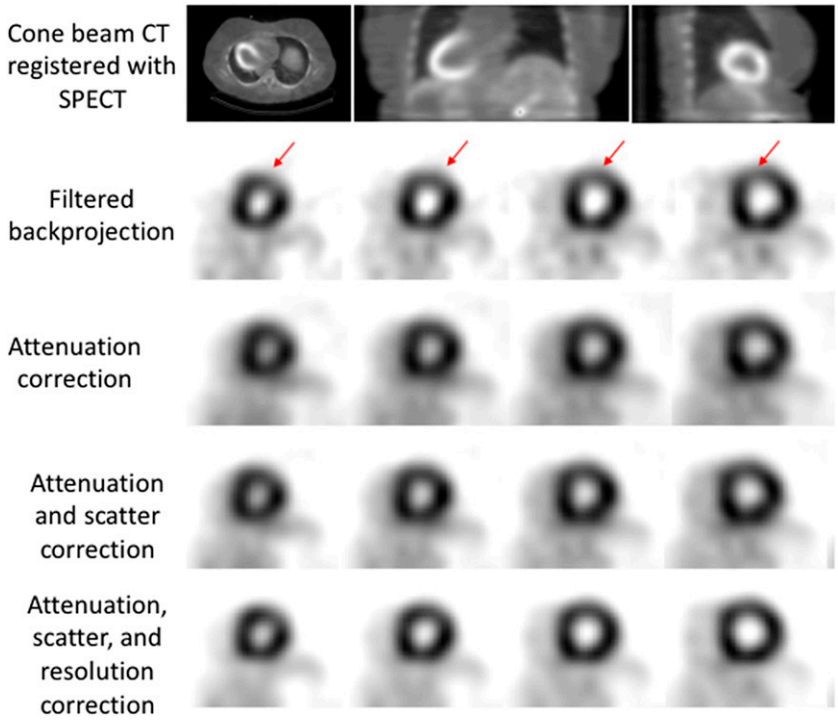

The key feature of an iterative reconstruction algorithm is that one starts with an initial estimate of the internal and unknown radionuclide distribution. This estimate can be any distribution and is usually an image set with equal and constant voxel values. SPECT projections are calculated from the initial estimate using a computer model of the imaging system described in the previous paragraph. The underlying assumption is that if the calculated projections match the measured projections, then the internal unknown activity distribution in the patient matches the estimate. Initially, these are most likely non-agreeing, so the initial estimate needs to be modified. Therefore, updates are made in the estimate based on a comparison between calculated projections of the estimate using the physics of the imaging process and the measured projections. By backprojection, the deviations between these two projection sets finally form an error image of weighting factors that is used to update the initial image estimate. This procedure is placed in an iterative loop in which the calculated and measured projections are compared until the deviation is smaller than a selected criterion (convergence has been reached). Hence, when this happens, the reconstruction loop is stopped. In practice, with noisy projection data, the iterative reconstruction procedures are stopped after only a small number of iterations, since the noise in the final image tends to increase for large number of iterations. Figure 2 shows a flowchart of the major steps in the iterative algorithm. The most popular iterative reconstruction algorithm implemented is ordered subset expectation maximization (OS-EM)[9] due to the speed with which it reaches a good estimate of the activity distribution. One potential problem associated with the method is that it does not theoretically converge to a single solution. Instead, it starts to cycle through different solutions instead of converging to only one.[10] The number of solutions will then be equal to the number of subsets. However, in most cases, the objects of interest in clinical imaging are smooth in their shapes so that the different solutions are closely related to each other and therefore, this property of the method is not a major drawback.

It should in this context be remembered that the iterative algorithm seeks a solution for the distribution of the radiopharmaceutical from a comparison between measured and calculated projections. The underlying assumption here is that the two projection sets have been created under the same conditions. However, if the computer model does not include all the physical effects such as non-homogeneous photon attenuation, contribution from scattered photons and blurring due to the collimator response, then the reconstructed image will not represent the true distribution even if the process reaches convergence. Therefore, compensation for these effects should in principle be made even for non-quantitative studies for which the absolute values of activity are of less importance. The compensation comes naturally in the iterative process since if a process is properly modelled in the forward/backward projector step (Figure 2), then this will automatically be a compensation for the physical effects. The following subsections will discuss the major physical effects that are important to consider.

Attenuation correction in single-photon emission CT

The use of CT information for attenuation correction led to an increased interest for this compensation method, since it was

Figure 2. A flowchart describing the different steps in an iterative reconstruction method: for the Maximum Likelihood Expectation Maximization (ML-EM) algorithm, the comparison is based on the ratio between the measured and the calculated projections. The principal difference between ML-EM and ordered subset expectation maximization (OS-EM) is that for OS-EM, the initial image is updated after a subset of projections have been processed, while for ML-EM the image is not updated until all projections have been processed. Although there are theoretical limitations with the OS-EM algorithm, the method has been successfully implemented for clinical applications and the improvement in speed of reading convergence is, as a rule of thumb, a factor equal to the number of subsets.

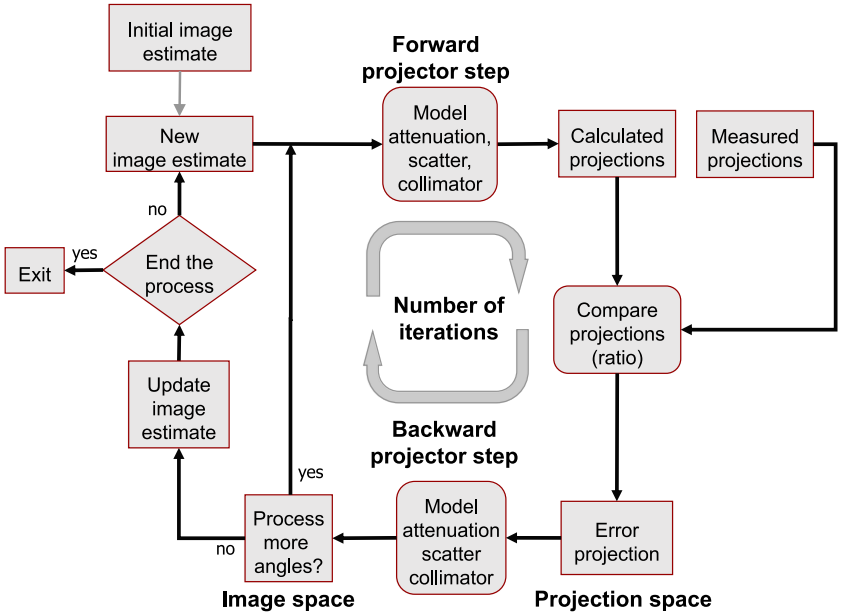

recognized that creating attenuation correction maps from external radionuclide sources mounted opposite the imaging detector imposed several serious limitations that were hard to overcome. Some of these limitations were (a) the additional operating cost of the decaying radioactive sources and the need to exchange them at regular intervals, (b) the problem with down scatter from the emission radionuclide that resulted in unwanted events in the transmission energy window, (c) poor resolution and (d) high image noise. The first GE Hawkeye 1 SPECT/CT system that created CT images for attenuation correction was superior when comparing with even high-quality diagnostic CT images produced by the current systems because the images were created for a long acquisition time so that breathing artefacts were not apparent. The images thus reflected the average attenuation of a long duration SPECT acquisition. Because of the coarse spatial resolution (3–4 mm), large slice thickness (10 mm) and long acquisition times (10 min), the quality of the resulting CT images was, of course, prohibitively poor for diagnostic applications.

Rapidly acquired, high-resolution diagnostic CT scans are, of course, of great value since they produce a high-definition anatomical map that can be used for a stand-alone radiological investigation. However, when combining the two systems, several issues need to be considered. First, it should be remembered that a SPECT projection is an acquisition averaged over many respiratory cycles. This means that motions will blur the image and the outline of a particular slice will define an average outline. When using rapidly acquired CT images for attenuation correction of such time-averaged slices, the CT image may not represent the internal structures very well because of the nearly instantaneous CT acquisition time. Secondly, the spatial resolution of the SPECT system is far coarser than that of CT. This means that if a high-resolution CT image set is used to compensate for attenuation, there is a potential risk of artefacts at boundaries between different attenuating tissues because of the spill-out of events due to the limited spatial resolution of the SPECT system. Often, this effect is reduced by smoothing the CT images with a Gaussian kernel that results in a spatial resolution of the CT images comparable with the spatial resolution of the SPECT images (which depends mainly on the collimator characteristics). Thirdly, depending of the acquisition parameters (voltage and mAs) the CT image may not be optimal for attenuation correction and the scaling from the X-ray bremsstrahlung spectra to the specific photon energy used in SPECT may not be optimal. When using CT only for attenuation correction, the so-called low-dose protocols can be used that are optimized for the purpose of compensation including a longer scanning time to average the respiratory movements and matched spatial resolutions (matrix size and slice thickness).

Scatter correction in single-photon emission CT

Several different scatter correction methods have been proposed and explored by many for clinical use.[11] Siemens and GE have implemented some form of the dual-energy window method based on the estimation of scatter from additional energy windows for subtraction from projection data or used within iterative reconstruction methods as an additive term.[12] However, there have been suggested alternatives to these methods, since it is generally known that the distribution of scatter in additional lower scatter windows does not reproduce the scatter distribution in the main photo-peak energy window. An alternative is to use model-based scatter compensation that does not rely on additional energy window data collection. Instead, it models the scatter in the main photo-peak energy window by using pre-calculated scatter kernels or in real-time calculates the scatter based on theoretical cross-sections of first-order scattering. Philips has implemented a version of the effective scatter source estimator method, originally developed by Frey and Tsui.[13]

Collimator response corrections

Most commercial systems in use offer some compensation for the limited spatial resolution due to the collimator design. These methods are generally implemented in the iterative reconstruction algorithm and model the depth-dependent blurring caused by photons that reach the detectors by an increased number of neighbouring holes, as the source is moved away from the collimator surface. Although the total number of counts for a parallel-hole collimator remains the same within the clinical volume of a SPECT acquisition, the spatial distribution of the counts will differ. Therefore, spill-in and spill-out from and to neighbouring voxels can occur when evaluating the counts in specific regions of interest. The model in the forward and backward projectors in principle treats all counts coming from the same distances separately. Before summation to the final projections, the separate images are filtered by a point spread function with a width that matches the resolution in a particular plane. The point spread functions can simply be Gaussian functions, which mainly mimic the geometrical component of the collimator response but can also include components from penetration and scatter in the collimator, which occur when using radionuclides that emit higher energies, such as ^{131}I or bremsstrahlung photons from ^{90}Y.

Partial volume correction

An extension of collimator response correction is partial volume correction. The effect of partial volume is an apparent reduction of the radioactive count density/X-ray density that occurs when an organ/tumour/defect only partially resides within the "sensitive volume of the imaging instrument (in space or time)".[14–19] From the review of Erlandsson et al,[19] it is clear that an extensive body of work exists in an effort to minimize the partial volume effect. The main aim of partial volume correction (as well as resolution correction) is to improve the quantitative accuracy of the structure under investigation. A diagnostic CT produces a very large fluence of X-ray photons that pass through a patient. To reduce the partial volume effect in this case, one only has to increase the sampling frequency (by reducing the voxel size and slice thickness). Projections from SPECT acquisitions, however, generally inherent limited count statistics due to the low sensitivity (registered counts per unit activity or cps/MBq) of the camera. Therefore, in SPECT, and owing to its relatively large voxel sizes, one has to rely on methods that "move" counts back to where they belong or methods that determine the mixture of different structures within an imaging voxel. Contrast-enhanced diagnostic CT images, sequentially acquired with SPECT/CT, can be used to accurately identify structures (tumours, organs etc.) at a high sampling frequency and determine the mixture when downsampling to the SPECT voxel size.[20]

Figure 3. Comparison of Monte Carlo-simulated ^{99m}Tc energy spectrum for a cadmium–zinc–telluride camera (left) and a conventional NaI(Tl) single-photon emission CT camera (right):[21] the phantom that has been simulated is an elliptical 30 × 22-cm water phantom with a cardiac insert. The scatter (photon interactions in the phantom) and primary (no photon interactions in the phantom) are also displayed as a separate energy spectrum.

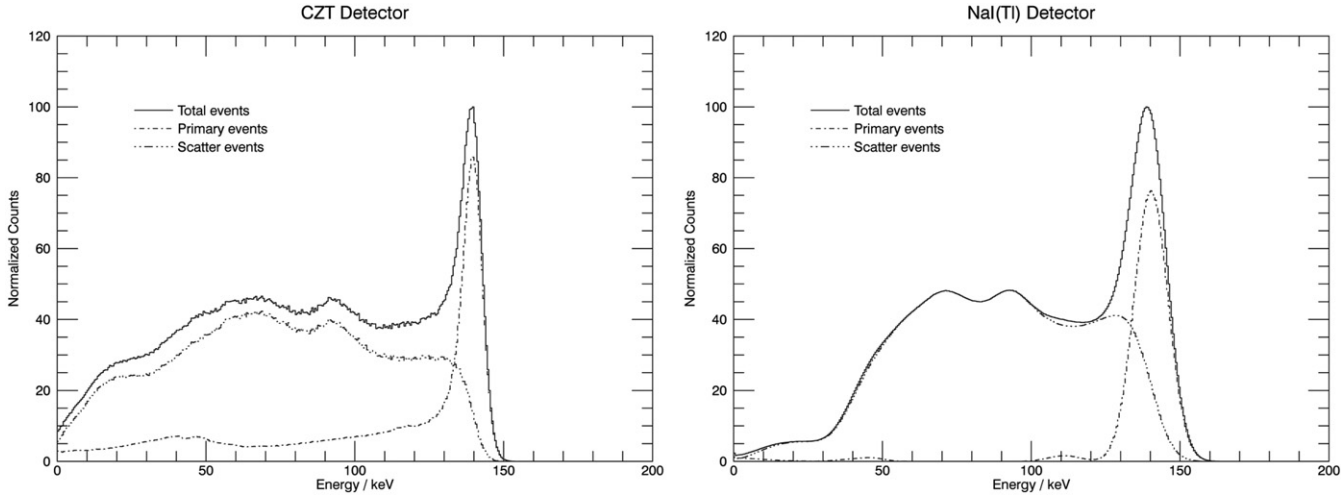

Motion problems and corrections

Acquisition times for conventional SPECT/CT systems vary and can be longer than 30 min. In all cases, two sets of data are acquired—the SPECT, which takes most of the time, and the CT, either before or after the SPECT. Patient body motion can occur during both the SPECT and CT portions of the study, but also during the transition from one to the other. For the latter, all manufacturers offer registration tools to manually register the SPECT and CT. Motion during the CT portion of the acquisition is usually minimized owing to short scan times as well as breath-holding by the patient when a diagnostic CT (2–16 slice) is used. Tidal breathing is recommended for the BrightView XCT from Philips. All manufacturers have some form of motion correction for SPECT using the consistency of the projections. These algorithms work best for small and simple motions. Most clinics will still repeat the acquisition when excessive body motion is present. With the improvement in SPECT spatial resolution over the past two decades, it now becomes imperative to consider the effects of respiratory motion.

NEW SINGLE-PHOTON EMISSION CT SYSTEMS BASED ON SOLID-STATE MATERIALS

NaI(Tl) is a scintillation material that has been in use for many years, is readily available, cost effective and still the predominantly used detector material in SPECT systems. The principal characteristic of scintillators is that the absorbed photon energy is converted to visible light in proportion to the deposited energy. The light is detected by PMTs, converted to electrons at the cathode surface of the PMTs and attracted to a sequence of dynodes to create an avalanche of electrons that results in an electrical signal which is further processed to supply energy and positional information. Because of the many steps involved, the uncertainty in the measured energy signal is quite large resulting in an energy resolution in the order of 10% full width at half maximum at 140 keV. Furthermore, a large number of PMTs are needed to determine the location of the interaction in the crystal and therefore, the scintillation camera head is quite large and requires sophisticated tuning methods so that all PMT provide similar amplitude signals for the same imparted energy. Recently, commercial SPECT systems based on cadmium–zinc–telluride (CdZnTe or simply CZT) have been introduced. CZT is a solid-state detector material with a density of 5.78 g cm^{-3} that generates signals from the collection of induced charge created by the ionizations from photoelectric interactions or Compton scattering. The induced charges are collected by individual anodes, since a high voltage is applied between the front surface (the cathode) and the pixelated anodes. Each anode therefore acts as an individual detector. There are two effects that make the characteristics of CZT detectors different from that of NaI(Tl). First, there is a possibility that the created electron-hole pairs can recombine during the charge diffusion process. This means that some of the electron-hole pairs will be lost and because there is an assumed proportionality between the absorbed energy and the number of created electron-hole pairs, the total measured energy will be reduced. The second effect is that the cloud of induced charge created by an interaction will also diffuse laterally along the transportation direction of the electric field. This diffusion can be described by a three-dimensional (3D) Gaussian distribution with a standard deviation that depends on the applied voltage and the depth of interaction. The result can be either a loss of induced charge due to the gap between the anodes or that charges are shared by anodes located nearby. The two effects, described above, lower and divide the detected energy and result in a characteristic tail below the photo-peak (Figure 3).[21]

Although they are not SPECT/CT systems, it can be worth mentioning in this context that dedicated molecular breast imaging is available commercially from GE Healthcare that uses CZT technology system (GE Discovery NM750b). A hand-held CZT camera with a matrix size of 32 × 32 (four CZT modules) that is designed mainly for visualization of sentinel lymph

node locations is manufactured by Crystal Photonics GmbH, Berlin, Germany.

Cadmium–zinc–telluride single-photon emission CT cameras for cardiac applications

Two systems based on the same CZT technology and dedicated to cardiac perfusion SPECT studies are at present commercially available. The first clinical system, introduced in the market, was the D-SPECT (Spectrum Dynamics, Caesarea, Israel) and this was followed later by the Discovery NM 530c (GE Healthcare, Haifa, Israel). Both systems have a C-shaped gantry that contains multiple detectors. The number of detectors is, however, different between the systems. The GE Discovery NM 530c has 19 stationary detectors equipped with pinhole collimators and arranged as 3 rows oriented perpendicular to the patient long axis. Nine detectors are located in position along a transaxial section and distributed around 180°. The other detectors are tilted and positioned as two groups of five detectors on each side of the main row of detectors. The D-SPECT has 10 CZT detectors where each is equipped with a parallel-hole square-hole collimator, made of tungsten, and where each detector swivels around its own axis to acquire an optimized number of projection angles. Figure 4 shows two sketches of how the detectors are positioned in the camera gantry of each camera. Both systems have detectors composed of four 16×16-pixel CZT modules of 5-mm thickness. The detectors for GE Discovery NM 530c are arranged as 2×2 modules with a total of 32×32 pixels, while the D-SPECT uses 1×4 modules as a 16×64-pixel arrangement. The pixel size for CZT modules is 2.46 mm and corresponds in a way to the intrinsic resolution which in conventional NaI(Tl) camera is in the order of 3.5 mm (depending on the crystal thickness).

The major advantages of these new CZT modules are the small size of the CZT module and the absence of PMTs, which allows for a compact camera but still with multiple detectors. This means that it is possible to increase the overall system sensitivity significantly (around 640 $MBq^{-1}\,s^{-1}$ for a source in air for the 530c system and 400 $MBq^{-1}\,s^{-1}$ for the D-SPECT system) as compared with, for example, the dedicated cardiac Ventri™ camera (GE Healthcare, Haifa, Israel), which has a system sensitivity of about 200 $MBq^{-1}\,s^{-1}$. The improvement in sensitivity can either be used to reduce the acquisition time of a given administered activity or the reverse or for improving the statistics in the acquired projections and thereby reducing the need for post-filtering. In the study by Oddstig et al,[22] they showed that the when using the CZT camera (GE NM 530c), the total effective dose could be decreased from 9.3 to 5.8 mSv by decreasing the administered activity from 4 to 2.5 MBq per kilogram body weight while keeping almost the same image quality. The SPECT spatial resolution is about 6.1 mm for the 530c system and 8 mm for the D-SPECT at 10 cm.[23] Also, there is the possibility to perform fast dynamic SPECT with both these systems, since all projections are acquired simultaneously. An example of improvement in both spatial resolution and image contrast is shown in Figure 5. The particular SPECT system for this example is the GE NM 530c system.

Full-sized cadmium–zinc–telluride single-photon emission CT/CT cameras

The newest CZT technology is the GE Healthcare full-size CZT-based SPECT/CT system (Discovery NM/CT 670 CZT), which is designed mainly for ^{99m}Tc, ^{201}Tl, ^{123}I, ^{133}Xe and ^{177}Lu isotopes. The system is based on the gantry of the two-headed GE Discovery NM/CT 670 Pro system, but the NaI(Tl) crystals and PMTs are replaced with CZT detectors. Each of the CZT module

Figure 4. A sketch is showing the location of the detectors in the GE NM 530c cadmium–zinc–telluride (CZT) single-photon emission CT (SPECT) system and the D-SPECT system: (a) for the GE system, there are nine detector locations of which five have three CZT blocks (two blocks of (b) each side of the centre slice location) and the other four have only the centre CZT block. (c) All detectors look at the same centre of rotation point where the heart should be positioned. The D-SPECT system has parallel-hole collimators and the 10 detectors are swivelled back and forth during the study in order to increase the number of projections.

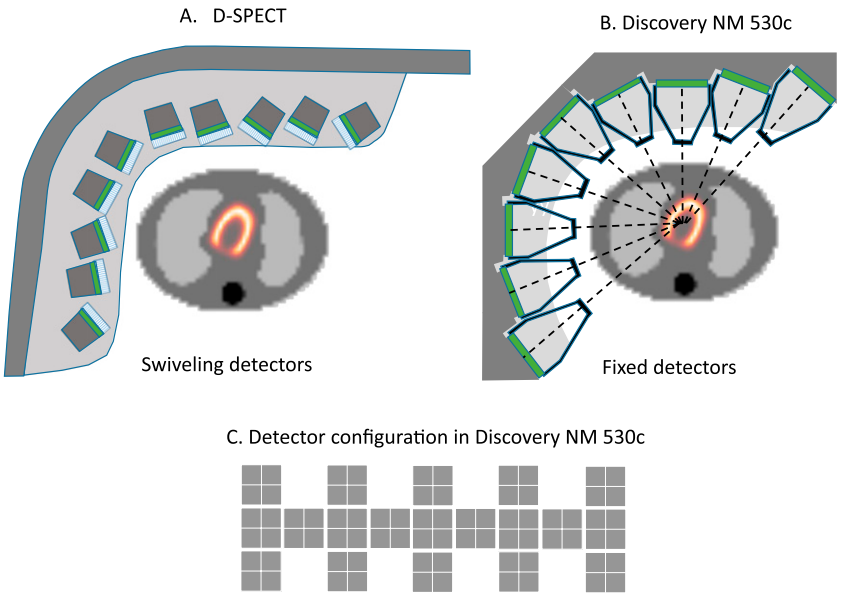

Figure 5. A comparison of a myocardial perfusion study obtained from the NM 530c cadmium–zinc–telluride (CZT) camera and a conventional NaI(Tl)-based camera: the NaI(Tl) camera acquired data in 15 min and with an administered activity of 925 MBq, while the CZT camera acquired data in 3 min with an administered activity of 185 MBq. [Courtesy Aharon Peretz, GE Healthcare, Haifa, Israel].

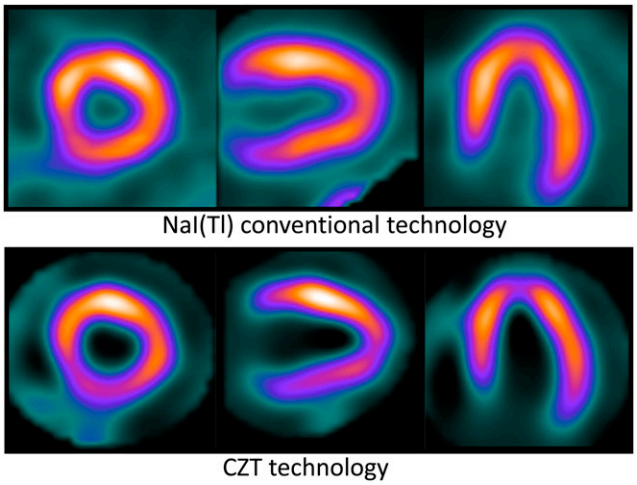

covers an FOV of $3.96 \times 3.96\,cm^2$, and there are 130 CZT modules per camera head. Figure 6 shows an image of the new full-sized CZT module package to the left and an image of the whole camera to the right.

For current users of the Discovery 670 Pro system, the modular design of this camera will allow for an upgrade to the Discovery 670 CZT by replacing the two detector heads. The detector area (39×51 cm) is smaller than that of a regular 670 camera based on the NaI(Tl) crystal, but the effective FOV is actually 25% larger owing to the lack of edge effects that distort the image and therefore makes this part of the camera field not useful. This means that data acquired in the whole FOV camera can be used. The detector frame is also reduced from 7.5 to 2.5 cm with the advantage of allowing for a more central positioning of the head with less shoulder interference when performing head and neck SPECT studies. This may improve the acquired spatial resolution for this specific acquisition protocol. The collimators are made of lead with square holes and the septa are registered to the gaps between the anodes of the CZT detector. This is a potential problem where the design of the collimator is not independent of the detector. Also here, the pixel size of the image is fixed and measures $2.46\,mm^2$. This provides a corresponding intrinsic spatial resolution of 2.46 mm at the face of the collimator, which is about 1.5 mm less than that of conventional scintillation camera systems. The energy resolution for 140-keV photons measured approximately 6.3% full width at half maximum at 140 keV according to the vendor. Since each anode in the CZT module acts as a separate independent detector, resolving time losses at high count rates are less as compared with traditional technology (1.4-fold higher count rate performance). The current version of the system includes only a low-energy ultrahigh-resolution collimator.

Figure 7 displays a comparison between a bone SPECT image obtained by a CZT camera and a conventional NaI(Tl) camera. Acquisition time was 8 min.

CLINICAL SINGLE-PHOTON EMISSION CT BASED ON MULTIPLE PINHOLES

The MILabs BV company in Utrecht, Netherlands, have recently announced their development of a clinical camera for the brain, and paediatric SPECT and envisage SPECT with an extended FOV called G-SPECT. It is designed as a full-ring stationary SPECT system with the capability of performing clinical imaging with a spatial resolution in the order of approximately 3 mm. The company also claims a unique capability of providing good-quality imaging studies but with a significantly lower administered activity due to the improved overall system sensitivity. The SPECT system will also be able to perform imaging of fast tracer dynamics. The inspiration for the clinical SPECT camera has been taken from the design of their U-SPECT pre-clinical μ SPECT system. The system consists of 9 large FOV cameras using $595 \times 472\text{-}mm^2$ NaI(Tl) scintillation crystals and the system has an interchangeable nonagon-shaped collimator that contains 54 pinhole apertures which thus results in 54 projections around the object acquiring data simultaneously. The company initial results, published on their web page, were obtained with a collimator with a bore diameter of 398 mm, but the plans are also to introduce a second larger bore collimator kit that will enable total-body and high-resolution cardiac imaging. SPECT images are reconstructed from list-mode data

Figure 6. Photographs of the new full-size field-of-view cadmium–zinc–telluride (CZT) detector system (a) that is included in the new NM/CT 670 CZT camera (b).

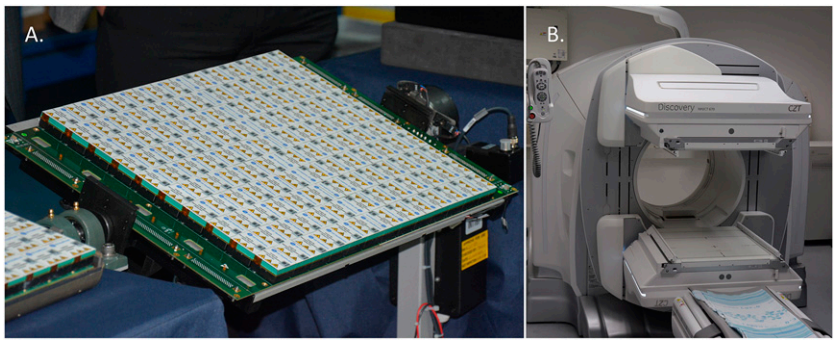

Figure 7. A comparison of bone scan coronal images obtained from the new NM/CT 670 cadmium–zinc–telluride camera and an ordinary NaI(Tl)-based NM/CT 670 Pro camera. The improved contrast that is partly due to reduced scatter contribution can be noted. [Courtesy Aharon Peretz, GE Healthcare, Haifa, Israel].

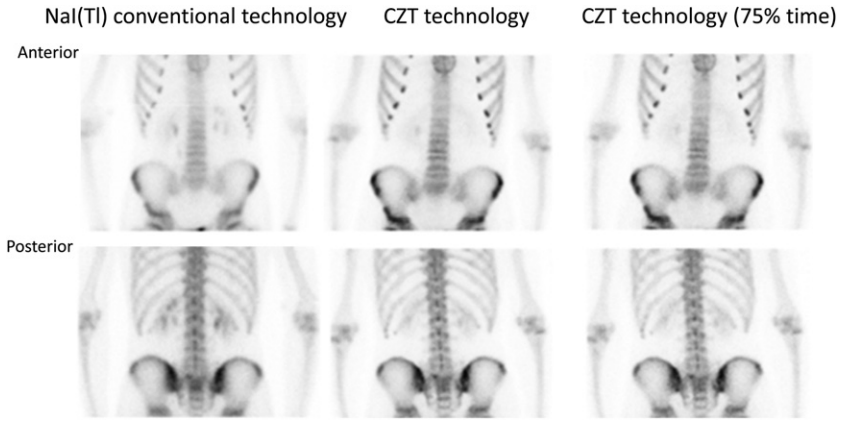

using a model-based 3D OS-EM reconstruction algorithm[24] that utilizes response function modelling of the system resolution and position-dependent sensitivity to improve resolution (Figure 8).

To demonstrate the improvement due to the novel design in terms of spatial resolution, the company have published images of the G-SPECT, where they compare their system with a commercial state-of-the-art Siemens dual-head SPECT camera equipped with low-energy high-resolution parallel-hole collimators using their OS-EM reconstruction (Flash3D) with resolution recovery.[25] The source activity filled in a Derenzo hot rod phantom was the same and the scan time was 15 min (Figure 9). MILabs researchers also claim that it may be possible with the new SPECT system to acquire dynamic image projections with a time interval of <10 s for focused scans and approximately 1 min when imaging the entire brain.

The prototype is not yet equipped with a CT, so image fusion and attenuation correction are most likely made by mathematically registered CT images. It should again be pointed out that at the moment of writing, this SPECT system was not released in the market; but, the authors of this review feel it still might be of interest to the readers.

CLINICAL APPLICATIONS USING SINGLE-PHOTON EMISSION CT/CT

Clinical reviews of applications of SPECT/CT have been compiled and published in several publications. The International Atomic Energy Agency published, in 2008, a book entitled "Clinical applications of SPECT/CT: new hybrid nuclear medicine imaging system",[26] which is available free for download and is an overview of the SPECT/CT technology and covers the status of SPECT/CT imaging, the role in the clinical management and possible future trends in development. Another book is "Clinical applications of SPECT-CT",[27] which reviews SPECT/CT in the diagnosis and therapy planning of benign and malignant diseases. Other review articles of clinical applications have been published.[1,28–31] Among these, Bailey and Willowson[32] have published an evidence-based review of the use of quantitative SPECT/CT.

Figure 8. A computer-rendered image of the new G-single-photon emission CT (SPECT) system announced by MiLabs. [Courtesy Freek Beekman, Delft University of Technology, Netherlands].

Figure 9. The image is showing a comparison between the G-single-photon emission CT (SPECT) and a Siemens Symbia system using a high-resolution phantom: the same acquisition time and activity (30 min and 22.5 MBq) have been used in both measurements. G-SPECT was reconstructed with a voxel-based ordered subset expectation maximization algorithm and Siemens Symbia was reconstructed with Flash3D. [Courtesy Freek Beekman, Delft University of Technology, Netherlands].

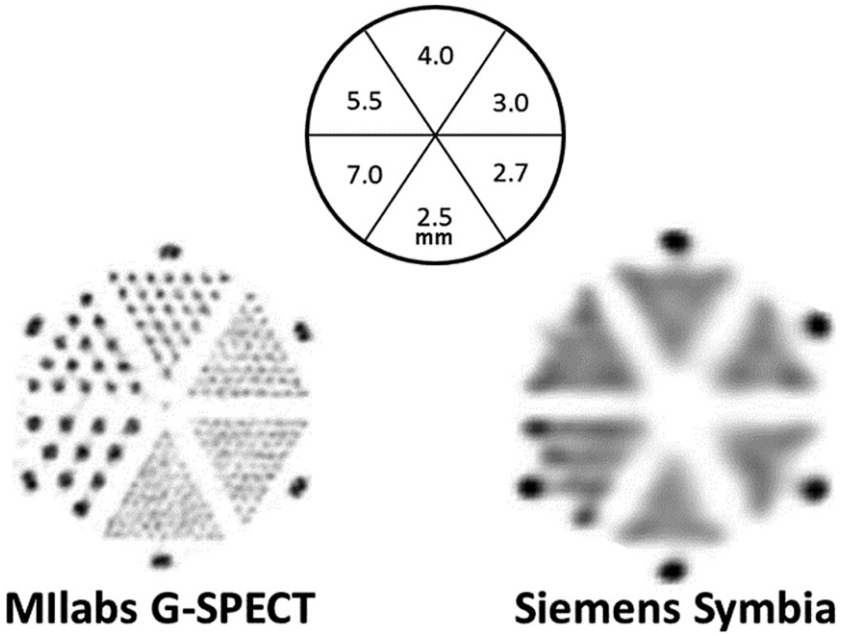

Lung single-photon emission CT/CT

The traditional way of evaluating possible pulmonary emboli has been to acquire planar views in different projections and compare studies representing air ventilation with blood perfusion. The group at the Lund University Hospital[33] pioneered the introduction of SPECT and especially the calculation and displaying of ventilation/perfusion quotient images by normalizing the counts in the ventilation image to the perfusion image and from this calculating the Ventilation/Perfusion quotient images. According to Bajc and Jonson,[34] the method has an excellent sensitivity and specificity and can be performed in all patients with a low radiation dose. A complete study can be made within 20 min. They conclude that the outstanding qualities make it qualified as a primary diagnostic method for pulmonary emboli.

^{99m}Tc and ^{201}Tl myocardial perfusion studies

Myocardial perfusion imaging (MPI) is one of the backbones of nuclear medicine and probably the first to benefit from the development of SPECT/CT; however, many clinicians and scientists involved in MPI appreciated the importance of attenuation and scatter correction prior to the availability of this technology[35–40] using transmission imaging.[2] It was also long realized that resolution compensation[36,40] should be part of the solution to improve MPI and even to reduce injected activity.[41] It has been shown in an Receiver operating characteristic study that compensating for all physical degradations, stress MPI has a significantly better area under the curve than when filtered backprojection is used in both rest and stress MPI.[40] With all the major vendors now offering SPECT/CT equipment with either low-end diagnostic CTs (Siemens, GE) or low-dose CBCT (Philips), these compensation techniques (photon attenuation, scatter and collimator resolution) are greatly enhanced owing to the improved quality of the attenuation maps. Furthermore, an additional value is added enabling clinicians to perform calcium scoring[42] as well as CT coronary angiography[43] in sequence with SPECT MPI. CT coronary angiography in combination with MPI also makes partial volume compensation possible,[19,20] and absolute blood flow measurements might not be far in the future[44,45] using technologies such as the GE Discovery 530c. The simultaneous acquisition of projections also makes respiratory motion estimation and compensation without respiratory motion tracking possible.[46]

A note of caution is necessary regarding the differences in durations of the SPECT and CT portions of an MPI acquisition. As discussed in the section on "Attenuation correction in SPECT", the newer SPECT/CT systems have CTs with much faster scan times and are able to accommodate breath-hold protocols. These protocols can cause mismatches between the SPECT and CT even after manual registration owing to the uncorrected respiratory motion in SPECT, especially when large. A study by Pretorius et al[47] shows that >30% of patients have respiratory motion estimates >10 mm and a maximum of 25 mm during ^{99m}Tc stress MPI. Some cardiac CT protocols call for slow or tidal breathing during acquisition (Philips BrightView with CBCT); however, in the study just mentioned,[47] streak artefacts in the location of the diaphragm are visible when excessive breathing occurs. This is due to the short CT acquisition time of 60 s used for cardiac protocols, effectively dividing approximately 15 respiratory cycles (4 s/cycle) across 300 projections or 20 projections per cycle. Figure 10 gives example coronal slices of low-dose CBCT slices of two female patients with vastly different respiratory motions. The arrows point to some of the differences.

^{99m}Tc bone scanning

Bone scintigraphy generally has a very high sensitivity because of the increased bone turnover caused by tumour growth. The specificity of scintigraphy, however, is much lower. Planar images acquired in anterior and posterior views has been the standard scintigraphy method for many years. The method uses inherently 2D projections and does not explore the information of the source depth. Therefore, it is impossible in many situations to determine whether a possible lesion is located in the spine or in the thoracic cage (Figure 11). Römer et al[48] demonstrated in 2006 the usefulness of SPECT/CT compared with planar imaging or SPECT. In their study, they demonstrated that the use of SPECT/CT-correlated images provided a definite diagnosis in 92% of skeleton lesions otherwise classified as indeterminate on using only SPECT. In a recent article, de Zwart et al[49] showed SPECT/CT to have a potential of being more accurate than planar scintigraphy imaging, as it uses anatomical information of the CT to discriminate among the scaphoid, other carpal bones and bone bruises. They concluded that SPECT/CT is superior to planar bone scintigraphy in the detection of occult fractures and presents additional information about the injury site and localization of the fracture, and the method could potentially serve as a future reference standard for studies concerning scaphoid fractures. More information regarding SPECT/CT and orthopaedic practice can be found in the review by Scharf.[50]

Parathyroid imaging

Primary hyperparathyroidism is diagnosable by a routine serum calcium measurement and since the first successful surgery early in the twentieth century, the size of parathyroid adenomas has decreased significantly.[51] Coakley et al[52] in 1989 reported a new imaging technique using ^{99m}Tc-sestamibi instead of the then routine ^{201}Tl/^{99m}Tc-pertechnetate subtraction protocol and the two methods were shown to be at least similar[53] by the same group. The two ^{99m}Tc-sestamibi protocols currently in use have been shown to benefit from the availability of SPECT CT.[54,55] The first,[54] pre-operative ^{123}I/^{99m}Tc-sestamibi subtraction SPECT/CT, was more specific than subtraction SPECT alone, while in the second,[55] dual-phase ^{99m}Tc-sestamibi parathyroid scintigraphy, benefitted from the CT, improving both specificity and sensitivity when planar imaging was used in combination with SPECT/CT. Hindié et al,[56] in an excellent continuing education article, suggested the first method is better; however, they did not reference the work of Lavely et al.[55] The location of the parathyroid in the neck close to the transition to the more significant attenuation of the shoulders makes SPECT/CT even more useful, "cleaning up" the highly non-uniform radioactive distribution that can occur locally. Furthermore, it is well known that smaller adenomas[51] should be better visualized when all physical degradations are included, similar to other disease states.[57]

Standard uptake values

The concept of standard uptake values (SUVs) has frequently been used in PET for tumour staging by employing relative quantification of tumour uptake. Recently, a study was published that evaluated the clinical usefulness of SUV methodology in ^{99m}Tc-methylene diphosphonate SPECT/CT bone scans for the assessment of determining the response in prostate cancer treatment.[58] SUV is defined as the ratio between the activity concentrations in the tumour and the average activity concentration in the normal tissue (which in practice is estimated by the body concentration). For simplicity, the volume of the body is approximated by the weight of the body. To calculate SPECT SUV, a proper compensation for photon attenuation, scatter and collimator response is very important, since it is activity and activity concentration that are obtained from the images and then normalized to administered activity. SPECT SUV software is commercially available by Hermes Medical Solutions (Stockholm, Sweden).

Prostate cancer

Prostate cancer is one of the most common cancers in males, which leads to morbidity and mortality, and this makes imaging very important for staging and to determine the proper treatment. Presently, PET/CT is the method of choice for imaging and here choline has been used as a radiotracer. Prostate-specific membrane antigen (PSMA) has shown to be a promising new target for both diagnostic imaging as well as therapy. Lütje et al[59] have published a review on the clinical status for PMSA applications. They describe studies of PSMA ligands with SPECT/CT for ^{123}I and ^{99m}Tc and for PET/CT with ^{68}Ga and ^{18}F. Because of the increased frequency of incidence of this type of malignancy, it can be expected that SPECT/CT will play an important role at sites where PET/CT is not available. Reinfelder et al[60] recently presented their experiences with ^{99m}Tc-labelled PSMA inhibitor

Figure 10. Example low-dose coronal cone-beam CT slices through the heart (left) and oesophageal spine (right) regions of two female patients of similar size (body mass indexes approximately 35.0 kg/m^2). The patient at the top respiration was estimated as 2.6-mm left to right (x), 7.3 mm anteroposterior (y) and 21.0-mm head to feet (z), while the same estimated for the patient at the bottom came to 1.7, 1.7 and 5.9 mm, respectively. The arrows are placed where the images at the bottom are more clearly defined than that at the top owing to the differences in respiratory motion.

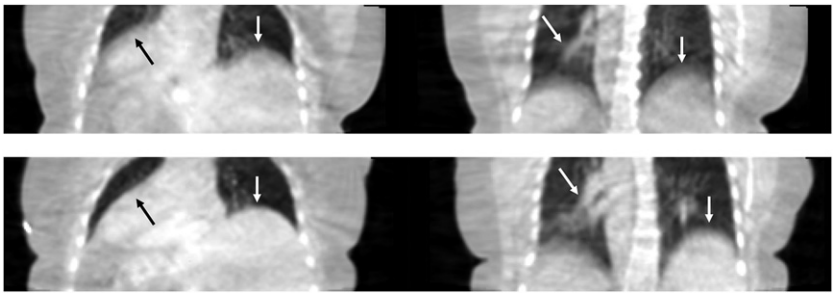

Figure 11. A comparison of images obtained with single-photon emission CT (SPECT)/CT (left two columns) and planar imaging (rightmost column): transversal and coronal images are shown for the two sections. The precise location of the lesion is hard to determine in the planar images owing to the lack of depth information, but from SPECT/CT it is clear that the lesion is located within one of the vertebras. Ant, anterior; Post, posterior.

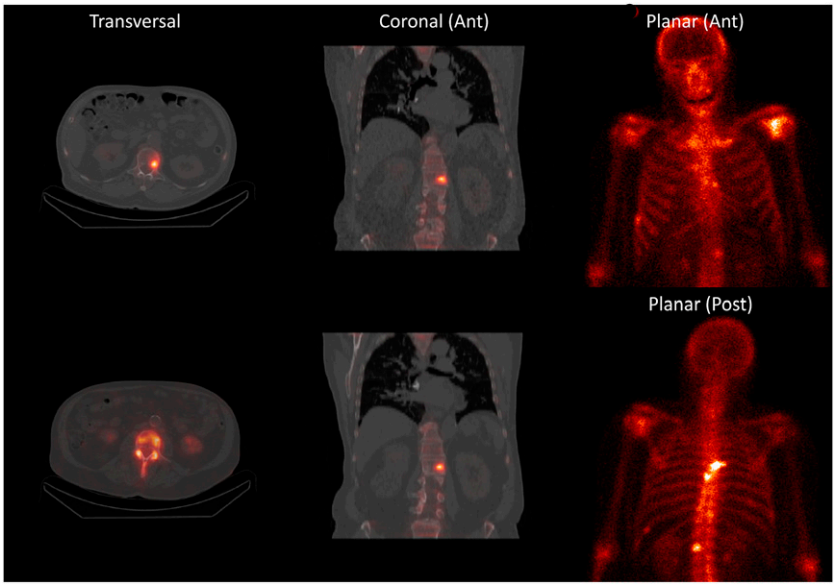

MIP-1404 detection of locally recurrent or metastatic prostate cancer. Other types of PSMA inhibitors, labelled with ^{123}I, have been studied by Barret et al.[61]

Single-photon emission CT/CT in radionuclide dosimetry

The number of nuclear medicine studies for dosimetry studies related to radionuclide therapy has increased significantly. Although PET is superior to SPECT regarding spatial resolution and sensitivity (counts per second per megabecquerel), there are not many potential positron-emitting radionuclides that are good candidates for radiotherapy because most of the positron emitters are short-lived. Dosimetry also relies on accurate quantification methods because the absorbed dose is directly calculated from quantitative SPECT/CT images. The ability to obtain patient-specific activity distribution together with patient geometry using a SPECT/CT system makes individual patient dosimetry possible. Examples of commercial packages are Dosimetry Toolkit (GE Healthcare),[62] Stratos® (Philips Medical Systems)[63] and VoxelDose[64] (DosiSoft, Cachan, France). A series of guidelines for quantitative SPECT have been published by the Medical Internal Radiation Dosimetry Committee including a generic description[65] and two nuclide-specific guidelines for ^{131}Iodine[66] and ^{177}Lutetium,[67] respectively.

Two major treatments employing dosimetry from SPECT/CT are the ^{90}Y selective internal radiation therapy and the treatment of patients with progressive metastatic neuroendocrine tumours with ^{177}Lu-DOTA-tyr3-Octreotate. Selective internal radiation therapy is increasingly used for treating inoperable primary or metastatic cancer in the liver. The treatment is accomplished by intrahepatic arterial administration of microspheres attached with ^{90}Y and these spheres are trapped in the vascular capillary tree owing to their size. The energy from the emitted β particles results in a lethal absorbed dose to the tissue that is proximal to the capillaries where tumour cells are located. A risk factor for the treatment is the shunting of ^{90}Y microspheres to the liver veins to be finally trapped in the lung capillary bed. A ^{99m}Tc-labelled macroaggregated albumin study is therefore performed prior to treatment in the same manner as the treatment with ^{90}Y spheres is performed to determine possible shunting. Quantitative SPECT/CT can be used for the ^{99m}Tc-labelled macroaggregated albumin administrations as part of a pre-therapy dose-planning procedure or for imaging the bremsstrahlung from ^{90}Y post-treatment in order to estimate the actual delivered absorbed dose.

The ^{177}Lu-DOTATATE treatments consist of a series of courses, in which a fixed amount of activity is administered to the patient. In order to determine the numbers of courses, the absorbed dose requires careful measurements and an accurate compensation for the previously mentioned physical problems. The treatment is continued until the cumulative absorbed dose reaches the limit for the kidneys. The absorbed dose is determined from multiple quantitative SPECT/CT or in combination with quantitative planar images. The treatment is based on a low-dose rate exposure over an extended time interval and reparation of cell damages may occur. Therefore, calculation of the biological effective dose is often the end point, since this parameter takes into account cell reparation during the irradiation time using a formalism based on the linear quadratic model for cell survival.[68]

RADIATION DOSE

The radiation doses received by patients from SPECT/CT examinations have been of concern for several years and serious efforts are been made to reduce the dose. In general, concerning risk of late carcinogenic diseases, one cannot say

anything about the absorbed dose to an individual. Instead, it is the general population exposed to a particular study that is of interest and where one should look at in order to find ways to reduce the dose. Of course, in general, the principle of avoiding unnecessary exposure should always hold true. Also, for certain populations with higher risk, such as pregnant females and young people, alternative investigations should be considered. New technologies such as dose modulation and iterative reconstruction methods can help reduce the dose. However, all new technologies are prone to taking time to garner widespread acceptance. Iterative reconstructed CT images with a different noise texture compared with filter backprojection methods make physicians uncomfortable and therefore, they might resist using such images for clinical evaluation of patients. A long-term training in reading these images might solve this problem. Another but similar example is the slow introduction and acceptance of CT attenuation-corrected SPECT myocardial perfusion images. It should also be kept in mind that the number of lives saved by early detection using radiological investigations such as SPECT and CT outnumber the potential risk of future late induction of secondary diseases. However, the risk and benefits should always be a taken into account.

CONCLUSION

It is clear that the introduction of combined SPECT/CT has improved the confidence with which many nuclear medicine studies are interpreted and has provided increased sensitivity. The availability of SPECT/CT may cause referring physicians to gravitate back to oncological applications traditionally performed by SPECT and planar scintigraphy that now are performed by CT, PET/CT or MRI. In combination with iterative reconstruction methods with proper modelling of photon attenuation, scatter and collimator resolution degradation, SPECT/CT systems will be very useful for studies requiring patient-specific dosimetry or dose planning and longitudinal studies, especially when longer half-life radionuclides not available in PET are needed.

FUNDING

Michael Ljungberg was in part supported by grants from the Bertha Kamprad Cancer Foundation. P Hendrik Pretorius, PhD, was in part supported by the National Heart, Lung, and Blood Institute of the National Institutes of Health under Award Number R01 HL122484.

REFERENCES

1. Mariani G, Bruselli L, Kuwert T, Kim EE, Flotats A, Israel O, et al. A review on the clinical uses of SPECT/CT. *Eur J Nucl Med Mol Imaging* 2010; **37**: 1959–85. doi: https://doi.org/10.1007/s00259-010-1390-8
2. King MA, Tsui BM, Pan TS. Attenuation compensation for cardiac single-photon emission computed tomographic imaging: part 1. Impact of attenuation and methods of estimating attenuation maps. *J Nucl Cardiol* 1995; **2**: 513–24.
3. Seo Y, Aparici CM, Hasegawa BH. Technological development and advances in SPECT/CT. *Semin Nucl Med* 2008; **38**: 177–98. doi: https://doi.org/10.1053/j.semnuclmed.2008.01.001
4. Hasegawa BH, Wong KH, Iwata K, Barber WC, Hwang AB, Sakdinawat AE, et al. Dual-modality imaging of cancer with SPECT/CT. *Technol Cancer Res Treat* 2002; **1**: 449–58. doi: https://doi.org/10.1177/153303460200100605
5. Tables of X-ray mass attenuation coefficients and mass energy—absorption coefficients from 1 keV to 20 MeV for elements $Z = 1$ to 92 and 48 additional substances of dosimetric interest. Gaithersburg, MD: National Institute of Standards and Technology. Available from: http://www.nist.gov/pml/data/xraycoef/
6. Anger HO. Scintillation camera. *Rev Sci Instrum* 1958; **29**: 27–33. doi: https://doi.org/10.1063/1.1715998
7. Bruyant PP. Analytic and iterative reconstruction algorithms in SPECT. *J Nucl Med* 2002; **43**: 1343–58.
8. Knoll P, Kotalova D, Köchle G, Kuzelka I, Minear G, Mirzaei S, et al. Comparison of advanced iterative reconstruction methods for SPECT/CT. *Z Med Phys* 2012; **22**: 58–69. doi: https://doi.org/10.1016/j.zemedi.2011.04.007
9. Hudson HM, Larkin RS. Accelerated image reconstruction using ordered subsets of projection data. *IEEE Trans Med Imaging* 1994; **13**: 601–9. doi: https://doi.org/10.1109/42.363108
10. Byrne CL. Accelerating the EMML algorithm and related iterative algorithms by rescaled block-iterative methods. *IEEE Trans Image Process* 1998; **7**: 100–9. doi: https://doi.org/10.1109/83.650854
11. Hutton BF, Buvat I, Beekman FJ. Review and current status of SPECT scatter correction. *Phys Med Biol* 2011; **56**: R85–112. doi: https://doi.org/10.1088/0031-9155/56/14/R01
12. Ogawa K, Harata Y, Ichihara T, Kubo A, Hashimoto S. A practical method for position-dependent Compton-scatter correction in single photon emission CT. *IEEE Trans Med Imaging* 1991; **10**: 408–12. doi: https://doi.org/10.1109/42.97591
13. Frey EC, Tsui BMW. A new method for modeling the spatially-variant, object-dependent scatter response function in SPECT. *IEEE Med Imaging Conf* 1996; **2**: 1082–6.
14. Hoffman EJ, Huang SC, Phelps ME. Quantitation in positron emission computed tomography: 1. effect of object size. *J Comput Assist Tomogr* 1979; **3**: 299–308.
15. Kessler RM, Ellis JR Jr, Eden M. Analysis of emission tomographic scan data: limitations imposed by resolution and background. *J Comput Assist Tomogr* 1984; **8**: 514–22. doi: https://doi.org/10.1097/00004728-198406000-00028
16. Pretorius PH, King MA, Pan TS, de Vries DJ, Glick SJ, Byrne CL. Reducing the influence of the partial volume effect on SPECT activity quantitation with 3D modelling of spatial resolution in iterative reconstruction. *Phys Med Biol* 1998; **43**: 407–20. doi: https://doi.org/10.1088/0031-9155/43/2/014
17. Muller-Gartner HW, Links JM, Prince JL, Bryan RN, McVeigh E, Leal JP, et al. Measurement of radiotracer concentration in brain gray matter using positron emission tomography: MRI-based correction for partial volume effects. *J Cereb Blood Flow Metab* 1992; **12**: 571–83. doi: https://doi.org/10.1038/jcbfm.1992.81
18. Hutton BF, Osiecki A. Correction of partial volume effects in myocardial SPECT. *J Nucl Cardiol* 1998; **5**: 402–13. doi: https://doi.org/10.1016/S1071-3581(98)90146-5
19. Erlandsson K, Buvat I, Pretorius PH, Thomas BA, Hutton BF. A review of partial volume correction techniques for emission tomography and their applications in neurology,

cardiology and oncology. *Phys Med Biol* 2012; **57**: R119–59. doi: https://doi.org/10.1088/0031-9155/57/21/R119
20. Pretorius PH, King MA. Diminishing the impact of the partial volume effect in cardiac SPECT perfusion imaging. *Med Phys* 2009; **36**: 105–15. doi: https://doi.org/10.1118/1.3031110
21. Pretorius PH, Liu C, Fan P, Peterson M, Ljungberg M. Monte Carlo simulations of the GE discovery alcyone CZT SPECT systems. *IEEE Trans Nucl Sci* 2015; **62**: 832–9. doi: https://doi.org/10.1109/TNS.2015.2433533
22. Oddstig J, Hedeer F, Jogi J, Carlsson M, Hindorf C, Engblom H. Reduced administered activity, reduced acquisition time, and preserved image quality for the new CZT camera. *J Nucl Cardiol* 2013; **20**: 38–44. doi: https://doi.org/10.1007/s12350-012-9634-6
23. Erlandsson K, Krzysztof K, van Gramberg D, Hutton BF. Performance evaluation of D-SPECT: a novel SPECT system for nuclear cardiology. *Phys Med Biol* 2009; **54**: 2635. doi: https://doi.org/10.1088/0031-9155/54/9/003
24. Branderhorst W, Vastenhouw B, Beekman FJ. Pixel-based subsets for rapid multi-pinhole SPECT reconstruction. *Phys Med Biol* 2010; **55**: 2023–34. doi: https://doi.org/10.1088/0031-9155/55/7/015
25. Beekman F, van der Have F, Goorden MC, Vaissier PEB, van Roosmalen J, During H, et al. G-SPECT-I: a full ring high sensitivity and ultra-fast clinical molecular imaging system with <3 mm resolution. Hamburg: EANM'15 Annual Conference; 13 October 2015.
26. Ahmadzadehfar H, Biersack HJ, eds. *Clinical applications of SPECT/CT: new hybrid nuclear medicine imaging system*. Vienna, Austria: International Atomic Energy Agency; 2008.
27. Ahmadzadehfar H, Biersack HJ, eds. *Clinical applications of SPECT-CT*. Berlin, Germany: Springer-Verlag; 2014. p. 304.
28. Huellner MW, Strobel K. Clinical applications of SPECT/CT in imaging the extremities. *Eur J Nucl Med Mol Imaging* 2014; **41** (Suppl. 1): S50–8. doi: https://doi.org/10.1007/s00259-013-2533-5
29. Jeong SY, Lee SW, Kim HW, Song BI, Ahn BC, Lee J. Clinical applications of SPECT/CT after first I-131 ablation in patients with differentiated thyroid cancer. *Clin Endocrinol (Oxf)* 2014; **81**: 445–51. doi: https://doi.org/10.1111/cen.12460
30. Hobbs SB, Hamon BW, Oates ME. A spectrum of SPECT/CT image fusion applications in daily clinical practice. *Clin Nucl Med* 2013; **38**: e336–41. doi: https://doi.org/10.1097/RLU.0b013e318281625a
31. Bhargava P, He G, Samarghandi A, Delpassand ES. Pictorial review of SPECT/CT imaging applications in clinical nuclear medicine. *Am J Nucl Med Mol Imaging* 2012; **2**: 221–31.
32. Bailey DL, Willowson KP. An evidence-based review of quantitative SPECT imaging and potential clinical applications. *J Nucl Med* 2013; **54**: 83–9. doi: https://doi.org/10.2967/jnumed.112.111476
33. Palmer J, Bitzen U, Jonson B, Bajc M. Comprehensive ventilation/perfusion SPECT. *J Nucl Med* 2001; **42**: 1288–94.
34. Bajc M, Jonson B. Ventilation/perfusion SPECT for diagnosis of pulmonary embolism and other diseases. *Int J Mol Imaging* 2011; **2011**: 682949. doi: https://doi.org/10.1155/2011/682949
35. Hendel RC, Berman DS, Cullom SJ, Follansbee W, Heller GV, Kiat H, et al. Multicenter clinical trial to evaluate the efficacy of correction for photon attenuation and scatter in SPECT myocardial perfusion imaging. *Circulation* 1999; **99**: 2742–9. doi: https://doi.org/10.1161/01.CIR.99.21.2742
36. Narayanan MV, King MA, Pretorius PH, Dahlberg ST, Spencer F, Simon E, et al. Human-observer receiver-operating-characteristic evaluation of attenuation, scatter, and resolution compensation strategies for (99m)Tc myocardial perfusion imaging. *J Nucl Med* 2003; **44**: 1725–34.
37. Hendel RC, Corbett JR, Cullom SJ, DePuey EG, Garcia EV, Bateman TM. The value and practice of attenuation correction for myocardial perfusion SPECT imaging: a joint position statement from the American Society of Nuclear Cardiology and the Society of Nuclear Medicine. *J Nucl Cardiol* 2002; **9**: 135–43. doi: https://doi.org/10.1067/mnc.2002.120680
38. Ficaro EP, Fessler JA, Shreve PD, Kritzman JN, Rose PA, Corbett JR. Simultaneous transmission/emission myocardial perfusion tomography. Diagnostic accuracy of attenuation-corrected 99mTc- sestamibi single-photon emission computed tomography. *Circulation* 1996; **93**: 463–73. doi: https://doi.org/10.1161/01.CIR.93.3.463
39. Corbett JR, Ficaro EP. Attenuation corrected cardiac perfusion SPECT. *Curr Opin Cardiol* 2000; **15**: 330–6. doi: https://doi.org/10.1097/00001573-200009000-00004
40. Pretorius PH, King MA, Gifford HC, Dahlberg ST, Spencer F, Simon E, et al. Myocardial perfusion SPECT reconstruction: receiver operating characteristic comparison of CAD detection accuracy of filtered backprojection reconstruction with all of the clinical imaging information available to readers and solely stress slices iteratively reconstructed with combined compensation. *J Nucl Cardiol* 2005; **12**: 284–93. doi: https://doi.org/10.1016/j.nuclcard.2005.01.012
41. Zafrir N, Bental T, Solodky A, Ben-Shlomo A, Mats I, Hassid Y, et al. Feasibility of myocardial perfusion imaging with half the radiation dose in obese patients using ordered-subset expectation maximization with resolution recovery software. *J Nucl Cardiol* 2013; **20**: 111–19. doi: https://doi.org/10.1007/s12350-012-9650-6
42. Rozanski A, Gransar H, Wong ND, Shaw LJ, Miranda-Peats R, Polk D, et al. Clinical outcomes after both coronary calcium scanning and exercise myocardial perfusion scintigraphy. *J Am Coll Cardiol* 2007; **49**: 1352–61. doi: https://doi.org/10.1016/j.jacc.2006.12.035
43. Rispler S, Keidar Z, Ghersin E, Roguin A, Soil A, Dragu R, et al. Integrated single-photon emission computed tomography and computed tomography coronary angiography for the assessment of hemodynamically significant coronary artery lesions. *J Am Coll Cardiol* 2007; **49**: 1059–67. doi: https://doi.org/10.1016/j.jacc.2006.10.069
44. Wells RG, Timmins R, Klein R, Lockwood J, Marvin B, deKemp RA, et al. Dynamic SPECT measurement of absolute myocardial blood flow in a porcine model. *J Nucl Med* 2014; **55**: 1685–91. doi: https://doi.org/10.2967/jnumed.114.139782
45. Liu C, Sinusas AJ. Is assessment of absolute myocardial perfusion with SPECT ready for prime time? *J Nucl Med* 2014; **55**: 1573–5. doi: https://doi.org/10.2967/jnumed.114.144550
46. Ko CL, Wu YW, Cheng MF, Yen RF, Wu WC, Tzen KY. Data-driven respiratory motion tracking and compensation in CZT cameras: a comprehensive analysis of phantom and human images. *J Nucl Cardiol* 2015; **22**: 308–18. doi: https://doi.org/10.1007/s12350-014-9963-8
47. Pretorius PH, Dahlberg ST, King MA. Investigation of respiratory motion compensation in a large population of patients undergoing Tc-99m cardiac perfusion SPECT/CT stress imaging. *J Nucl Med* 2016 **57**: 532.
48. Römer W, Nomayr A, Uder M, Bautz W, Kuwert T. SPECT-guided CT for evaluating foci of increased bone metabolism classified as indeterminate on SPECT in cancer patients. *J Nucl Med* 2006; **47**: 1102–6.
49. de Zwart AD, Beeres FJ, Rietbergen DD, Krijnen P, Schipper IB. Initial experience of SPECT/CT in the diagnosis of occult scaphoid fracture. *Acta Radiol Open* 2015; **4**: 2058460115602729. doi: https://doi.org/10.1177/2058460115602729
50. Scharf S. SPECT/CT imaging in general orthopedic practice. *Semin Nucl Med* 2009;

39: 293–307. doi: https://doi.org/10.1053/j.semnuclmed.2009.06.002
51. Almquist MB, Martensson H, Thier M, Nordenstrom E. Changing biochemical presentation of primary hyperparathyroidism. *Langenbecks Arch Surg* 2010; **395**: 925–8. doi: https://doi.org/10.1007/s00423-010-0675-5
52. Coakley AJ, Wells CP, O'Doherty MJ, Collins RE. 99mTc sestamibi: a new agent for parathyroid imaging. *Nucl Med Commun* 1989; **10**: 791–4. doi: https://doi.org/10.1097/00006231-198911000-00003
53. O'Doherty MJ, Wells P, Collins RE, Coakley AJ. Parathyroid imaging with technetium-99m-sestamibi: preoperative localization and tissue uptake studies. *J Nucl Med* 1992; **33**: 313–18.
54. Neuman DR, DiFilippo FP. Preoperative 123I/99mTc-sestamibi subtraction SPECT and SPECT/CT in primary hyperparathyroidism. *J Nucl Med* 2008; **49**: 2012–17.
55. Lavely WC, Goetze S, Friedman KP, Leal JP, Zhang Z, Garret-Mayer E, et al. Comparison of SPECT/CT, SPECT, and planar imaging with single- and dual-phase 99mTc-sestamibi parathyroid scintigraphy. *J Nucl Med* 2007; **48**: 1084–9. doi: https://doi.org/10.2967/jnumed.107.040428
56. Hindié EZ, Tabarin A, Rubello D, Morelec I, Wagner T, Hendry JF, et al. The role of radionuclide imaging in the surgical management of primary hyperparathyroidism. *J Nucl Med* 2015; **56**: 737–44. doi: https://doi.org/10.2967/jnumed.115.156018
57. Farncombe TH, Gifford HC, Narayanan MV, Pretorius PH, Frey EC, King MA. Assessment of scatter compensation strategies for Ga-67 SPECT using numerical observers and human LROC studies. *J Nucl Med* 2004; **45**: 802–12.
58. Mao JL, Zhai W, Lewis R, He W, Avondo J, Hacker M, et al. The clinical value of SUV measurements in 99mTC-MDP SPECT/CT bone scans in the evaluation of therapy response in prostate cancer patients with bone metastases. *J Nucl Med* 2015; **56**(Suppl. 3): 1789.
59. Lütje S, Heskamp S, Cornelissen AS, Poeppel TD, van den Broek SA, Rosenbaum-Krumme S, et al. PSMA ligands for radionuclide imaging and therapy of prostate cancer: clinical status. *Theranostics* 2015; **5**: 1388–401.
60. Reinfelder J, Kuwert T, Prante O, Wullich B, Hennig P, Beck M, et al. First experience with PSMA-SPECT/CT using a 99mTc-labeled PSMA inhibitor for patients with biochemical recurrence of prostate cancer. *J Nucl Med* 2015; **56**(Suppl. 3): 67.
61. Barrett JA, Coleman RE, Goldsmith SJ, Vallabhajosula S, Petry NA, Cho S, et al. First-in-man evaluation of 2 high-affinity PSMA-avid small molecules for imaging prostate cancer. *J Nucl Med* 2013; **54**: 380–7. doi: https://doi.org/10.2967/jnumed.112.111203
62. Mauxion T, Frey E. Quantitative comparison of dosimetry toolkit (DTK) and custom software for hybrid 2D/3D residence time estimation. *J Nucl Med* 2015; **56**(Suppl. 3): 102.
63. Grassi E, Fioroni F, Ferri V, Mezzenga E, Sarti MA, Paulus T, et al. Quantitative comparison between the commercial software STRATOS® by Philips and a homemade software for voxel-dosimetry in radiopeptide therapy. *Phys Med* 2015; **31**: 72–9. doi: https://doi.org/10.1016/j.ejmp.2014.10.002
64. Jackson PA, Beauregard JM, Hofman MS, Kron T, Hogg A, Hicks RJ. An automated voxelized dosimetry tool for radionuclide therapy based on serial quantitative SPECT/CT imaging. *Med Phys* 2013; **40**: 112503. doi: https://doi.org/10.1118/1.4824318
65. Dewaraja YK, Frey EC, Sgouros G, Brill AB, Roberson P, Zanzonico PB, et al. MIRD pamphlet no. 23: quantitative SPECT for patient-specific 3-dimensional dosimetry in internal radionuclide therapy. *J Nucl Med* 2012; **53**: 1310–25. doi: https://doi.org/10.2967/jnumed.111.100123
66. Dewaraja YK, Ljungberg M, Green AJ, Zanconico PB, Frey EC. MIRD pamphlet no. 24: guidelines for quantitative 131I- SPECT in dosimetry applications. *J Nucl Med* 2013; **54**: 2182–8. doi: https://doi.org/10.2967/jnumed.113.122390
67. Ljungberg M, Celler A, Konijnenberg MW, Eckerman KF, Dewaraja YK, Sjogreen-Gleisner K. MIRD pamphlet no. 26: joint EANM/MIRD guidelines for quantitative 177Lu SPECT applied for dosimetry of radiopharmaceutical therapy. *J Nucl Med* 2016; **57**: 151–62. doi: https://doi.org/10.2967/jnumed.115.159012
68. Gustafsson J, Nilsson P, Gleisner KS. On the biologically effective dose (BED)-using convolution for calculating the effects of repair: II. Numerical considerations. *Phys Med Biol* 2013; **58**: 1529–48. doi: https://doi.org/10.1088/0031-9155/58/5/1529